

Adsorbed Water Promotes Chemically Active Environments on the Surface of Sodium Chloride

Xiangrui Kong,* Ivan Gladich,* Nicolas Fauré, Erik S. Thomson, Jie Chen, Luca Artiglia, Markus Ammann, Thorsten Bartels-Rausch, Zamin A. Kanji, and Jan B. C. Pettersson*



Cite This: *J. Phys. Chem. Lett.* 2023, 14, 6151–6156



Read Online

ACCESS |



Metrics & More

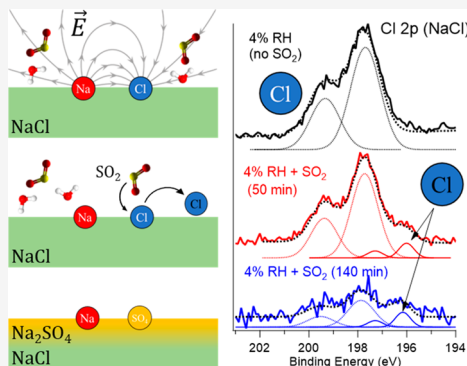


Article Recommendations



Supporting Information

ABSTRACT: Gas–particle interfaces are chemically active environments. This study investigates the reactivity of SO_2 on NaCl surfaces using advanced experimental and theoretical methods with a NH_4Cl substrate also examined for cation effects. Results show that NaCl surfaces rapidly convert to Na_2SO_4 with a new chlorine component when exposed to SO_2 under low humidity. In contrast, NH_4Cl surfaces have limited SO_2 uptake and do not change significantly. Depth profiles reveal transformed layers and elemental ratios at the crystal surfaces. The chlorine species detected originates from Cl^- expelled from the NaCl crystal structure, as determined by atomistic density functional theory calculations. Molecular dynamics simulations highlight the chemically active NaCl surface environment, driven by a strong interfacial electric field and the presence of sub-monolayer water coverage. These findings underscore the chemical activity of salt surfaces and the unexpected chemistry that arises from their interaction with interfacial water, even under very dry conditions.



Gas–particle interfaces are chemically active places,¹ especially when reversibly adsorbed water is present in equilibrium with water vapor.² For example, thermodynamic reactions that are normally disfavored have been found to spontaneously take place on salt surfaces that are being solvated by adsorbed water.² More generally, (salt) surfaces have special properties and chemical reactivities, but our holistic understanding is incomplete. Chloride salts, particularly NaCl, are common compounds on Earth and other planets.^{3–5} From a physicochemical perspective, NaCl plays an active role in our climate system, notably in aerosol growth that leads to cloud formation, as a result of its high hygroscopicity.⁶ Furthermore, NaCl can bind with water molecules to hydrohalite ($\text{NaCl}\cdot 2\text{H}_2\text{O}$),⁷ which serves as active ice nucleating particles (INPs).⁸ Nonetheless, chemically speaking, NaCl in its dry salt crystal form is generally considered to be unreactive, except for its surface, which can react with nitrogen oxides.⁹ Considering that the NaCl surface already exhibits surface-bound water at a quite low relative humidity (RH)¹⁰ and the potential that water may chemically activate the surface environment,² it is relevant to understand the physicochemical nature of NaCl surfaces in the presence of adsorbed water.

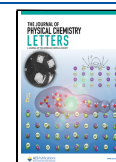
In this study, the NaCl surface chemical activity is investigated in conjunction with SO_2 gas uptake and the resulting transformations, which has a high relevance on the global scale given the considerable mixing of these two components. SO_2 is a common and important gas from both natural and anthropogenic sources,^{11,12} which is particularly

critical in aerosol science because SO_2 gas can be efficiently converted to sulfate (SO_4^{2-}). Sulfate is an important contributor to particulate matter formation during haze periods.¹³ Traditionally, sulfate formation mechanisms primarily include gas phase oxidation of SO_2 by OH radicals and aqueous oxidation of S(IV) by H_2O_2 , O_3 , organic peroxides, NO_2 , and O_2 catalyzed by transition metal ions in cloud/fogwater droplets.¹⁴ However, these mechanisms of oxidizing the precursor (SO_2) to sulfate are insufficient to explain observed sulfate concentrations, especially in cloud-free, polluted areas where highly concentrated aerosol plays a role,¹⁵ which leads to large discrepancies in chemical transport models.^{13,16} This contributes to radiative forcing uncertainty and the role of SO_2 therein, as shown in the latest Intergovernmental Panel on Climate Change (IPCC) report.¹⁷ When water is present on surfaces, surface catalysis mechanisms have been discovered to potentially have significant impacts on the sulfur chemistry of the atmosphere.^{2,15,18,19} Here, we investigate the heterogeneous pathway of SO_2 uptake and conversion on the NaCl surfaces. For comparison, another chloride salt, NH_4Cl , is used to examine

Received: April 11, 2023

Accepted: June 7, 2023

Published: June 29, 2023



the effects of a different cation and crystalline structure on the adsorption and chemistry. We combine surface-sensitive techniques [ambient pressure X-ray photoelectron spectroscopy (APXPS) and near-edge X-ray absorption fine structure (NEXAFS)] and first-principles molecular dynamics (FPMD) simulations to investigate the heterogeneous uptake and oxidation of SO₂ gas on the surfaces of NaCl and NH₄Cl.

In Figure 1, SO₂ uptake on NaCl and the evolution of the system are shown, including the photoemission spectra of

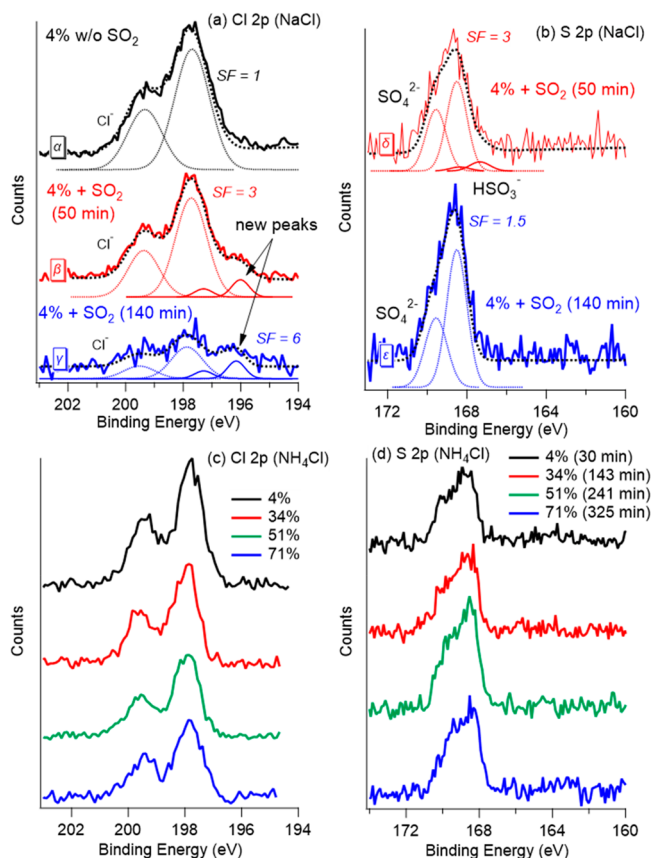


Figure 1. (a) Chloride 2p and (b) sulfur 2p XPS spectra measured at different exposure times (50 and 140 min) for 0.01 mbar of SO₂ on NaCl at a RH of 4%. The photon energy was set to 570 eV for sulfur XPS and 600 eV for chlorine XPS, which results in the same electron kinetic energy for sulfur and chlorine and, consequently, the same mean escape depths. The spectra are normalized by scaling factors (SFs), which are marked beside the spectra. The fitted peaks are presented as dotted and solid lines. (c) Chlorine 2p and (d) sulfur 2p XPS spectra measured at different RHs with 0.01 mbar of SO₂ exposure on NH₄Cl. The exposure time is indicated in the legend. The binding energy was aligned using aliphatic carbon at 284.8 eV as a reference. During the measurements of these spectra, water and SO₂ gases were present.

sulfur and chlorine species on NaCl and NH₄Cl surfaces at various relative humidities (RHs) and after different exposure times (50 and 140 min) to 0.01 mbar SO₂. On NaCl surfaces, the initial spectrum (spectrum α in Figure 1a, at a RH of 4%, without SO₂) shows a neat doublet fitted with two component peaks at binding energies (BEs) of 199.4 and 197.7 eV, respectively. These correspond to the chloride ions (Cl 2p electrons) in the NaCl crystalline structure.²⁰ After the NaCl surface is exposed to SO₂ for 50 min (spectrum β in Figure 1a), the Cl 2p intensity decreases noticeably (spectrum β is

scaled by a factor of 3). In addition, a new component emerges at a lower BE, which is fitted by a doublet with peaks at around 197.7 and 196.0 eV. At a longer exposure time (140 min), the chloride-related signal is mostly depleted (spectrum γ in Figure 1a, where a scaling factor of 6 is applied), but the new Cl doublet remains visible. This species is formed when SO₂ is dosed but never significantly grows, even as the original chloride doublet decreases substantially within 140 min of exposure time. A possibility is that this new doublet may correspond to an intermediate steady-state species on the surface, having balanced pathways for both formation and a sink; i.e., this species might be continuously formed and subsequently depleted, such as by escaping to the gas phase. The identification of this new Cl doublet is discussed in conjunction with theoretical results later.

Sulfur spectra are shown in Figure 1b. The spectrum δ shows that, after 50 min, both sulfate and bisulfite (HSO₃²⁻) doublets are observed on the surface (sulfate at 169.6 and 168.5 eV and bisulfite at 168.4 and 167.3 eV),^{21–24} showing the SO₂ uptake and transformation on the surface. After 140 min, the sulfate doublet grew further (note the lower SF applied in spectrum ϵ). In addition, the soft X-ray radiation used in the experiments also plays a role and accelerates the displacement of chloride by sulfate, as discussed in Figure S1 of the Supporting Information.

In contrast, the chlorine depletion and sulfur accumulation are limited on the other investigated chloride salt, NH₄Cl, even after long exposure times (>5 h) at various RHs (0–70%). Note that the different chemical reactivities of the two salts are not caused by the X-ray beam, because NH₄Cl received a higher dose than NaCl. Panels c and d of Figure 1 show that the sulfate and chlorine signals are relatively stable over a large span of RHs, and no additional chlorine doublet emerges. The difference between the results for NaCl and NH₄Cl salts shows that the NaCl surface is a more reactive environment for SO₂ uptake, sulfate formation, and chlorine replacement.

The observation that chlorine is depleted as sulfate production increases supports a hypothesis that the NaCl surface is transforming to a surface composed of sodium and sulfate, e.g., Na₂SO₄. To verify this, sodium and oxygen K-edge NEXAFS spectra were acquired and are shown in Figure 2. For fresh NaCl that was never exposed to SO₂, Figure 2a shows that its sodium NEXAFS has distinguishable peak features, as previously reported for crystalline NaCl.²⁵ After SO₂ exposure, the sodium NEXAFS spectra gradually change over time, toward a smoother line structure. For reference, the blue spectrum presents a pure Na₂SO₄ sample measured at a RH of 3%. After 5 h, the sodium NEXAFS spectrum has become very similar to the Na₂SO₄ reference spectrum, confirming that most sodium atoms are binding with sulfate instead of chloride on the surface. In addition, a “reverse” case is shown as the gray line, where the RH is reduced from 4 to 0% by stopping the water vapor supply. The RH drop does not induce any visible changes on the spectrum, suggesting that sulfate is stable at the surface. Moreover, sulfate remains stable under ultrahigh vacuum (UHV) conditions, because after being kept under UHV overnight, no sulfur depletion was observed.

The oxygen NEXAFS spectra (Figure 2b) show that there is almost no oxygen signal at a RH of 4% before the SO₂ dosage. The trace amounts are likely attributable to adsorbed water that cannot be removed from the drop cast samples under these conditions. When SO₂ is introduced, a sharp peak around 535 eV grows over time, which corresponds to oxygen in

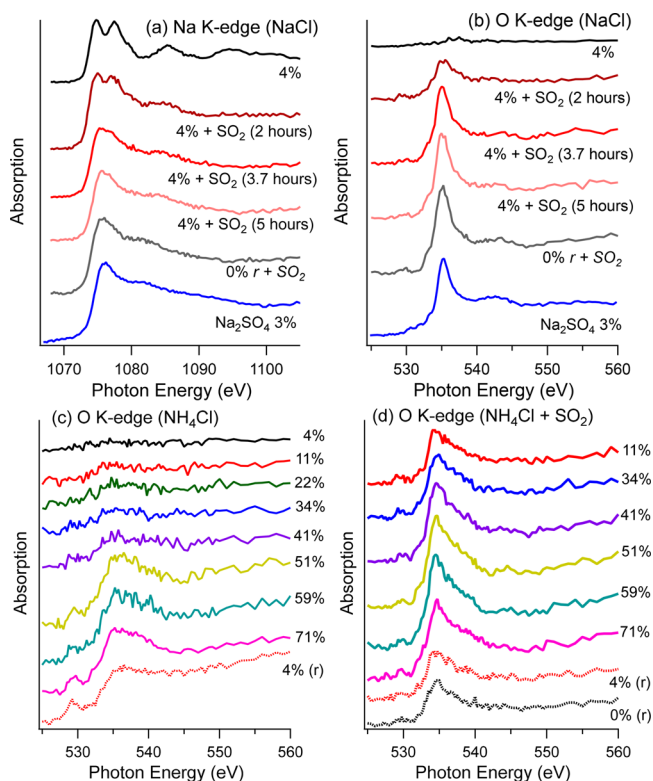


Figure 2. (a) Sodium K-edge and (b) oxygen K-edge NEXAFS measured at a RH of 4% with 0.01 mbar of SO_2 exposure on NaCl. Oxygen K-edge NEXAFS was measured on NH_4Cl at various RHs (c) without and (d) with 0.01 mbar of SO_2 exposure. A detailed comparison of panels c and d can be found in Figure S2 of the Supporting Information.

sulfate.^{23,26} Like the sodium NEXAFS spectra, after 5 h, the oxygen spectra show features similar to pure Na_2SO_4 . Again, a RH reduction does not affect the sulfate in the oxygen spectrum. Noticeably, around 543 eV, a new structure does appear that, according to the energy, likely originates from water bonded to sulfate.²³ This component is also maintained when the RH is reduced to 0%, indicating that strong bonds are formed.

To the contrary, the NH_4Cl surface is relatively robust to SO_2 exposure, independent of RH (panels c and d of Figure 2). In the SO_2 -free cases (Figure 2c), the oxygen NEXAFS shows that the surface is covered by adsorbed water when RH is

increased above 40%, and the water remains when the measurement is taken as the RH returns to 4% (possibly a hysteresis effect). When SO_2 is present (Figure 2d), oxygen NEXAFS shows a broad distribution already at a RH = 10%, which suggests the existence of a combination of adsorbed water and sulfate/bisulfite and highlights the synergetic effects of SO_2 and water uptake. However, the sulfur abundance on the NH_4Cl surface is stable over a wide RH range, as presented in Figure S3 of the Supporting Information. This implies that the NaCl surface is more active for SO_2 uptake than NH_4Cl at a RH of 4%.

Elemental ratios on the SO_2 -exposed NaCl surface are evaluated at two kinetic energies, and the results are shown in Figure 3a. All elemental ratios exhibit constant values between kinetic energies of 400 and 600 eV, which correspond to an electron inelastic mean free path (IMFP) of 1.2–1.6 nm in Na_2SO_4 and 1.5–2.0 nm for NaCl.²⁷ The constant ratios indicate homogeneous distributions along the probed depth. Reference elemental ratios for pure materials (NaCl and Na_2SO_4) are marked as dotted lines, and quantitative chemometric analysis (see details in the Supporting Information) shows that the composition of layers is likely complicated, i.e., a combination of NaCl, Na_2SO_4 , NaHSO_4 , and H_2SO_4 .

The elemental ratios for SO_2 on NH_4Cl are shown in Figure 3b as a function of RH. Some ratios, such as Cl/O, N/O, and Cl/N, decrease dramatically as RH increases and more water and SO_2 are expected to co-condense on the surface. The decreasing Cl/N ratio indicates that Cl^- is selectively surface-depleted or NH_4^+ is relatively surface-enriched, because the only source of these elements is the salt itself. However, because gas phase SO_2 can be taken up together with water vapor as RH rises, it is more likely that Cl^- is repelled from the gas–salt surface by competing anions, like SO_4^{2-} or HSO_4^- . It is interesting that, on other hydrated salts (e.g., $\text{MgCl}_2 \cdot 8\text{H}_2\text{O}$ crystal), the observed behavior is the reverse, with monovalent ions drawn toward the water–salt interface to complete their solvation shells, while divalent ions are pushed toward the gas phase interface.²³ The S/O ratio begins at 0.5 for RH = 0% as expected with only the SO_2 present but quickly decreases with the presence of water vapor and then remains steady around 0.33, suggesting comparable uptake of the gas phase H_2O and SO_2 . The only increasing trend shown in the figure is the S/N ratio, which rises together with RH as more SO_2 is taken up at higher RHs.

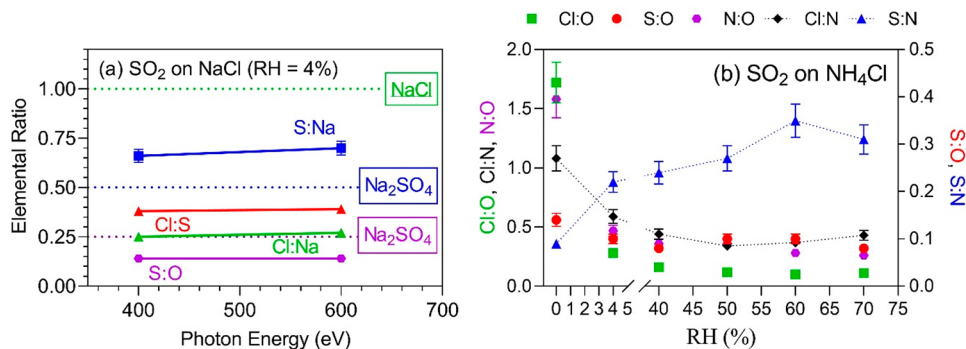


Figure 3. (a) Depth profile of elemental ratios of SO_2 -doped NaCl at a RH = 4%. The dotted lines show the elemental ratios of pure materials, as marked with boxes. The SO_2 exposure time was 2–2.5 h during the measurements. (b) Depth profile of elemental ratios on a SO_2 -doped NH_4Cl surface at various RHs. The measurement took about 8 h, and SO_2 was present.

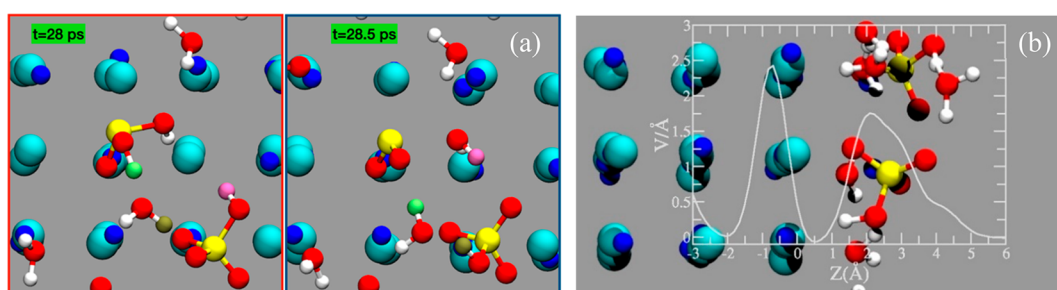


Figure 4. (a) Top view of a NaCl crystal showing the dehydration of H_2SO_3 into SO_2 . In green, brown, and pink, the H atoms are involved in proton transfer. (b) Average component of the electric field perpendicular to the interface, $E_z(z)$. A first peak is located in proximity to the interfacial NaCl crystal, and a second peak overlays the adsorbed water solution layer.

To better understand the surface environment of NaCl and how relevant adsorbent species behave, atomistic simulations at density functional theory (DFT) levels were performed. The first task was to identify the chlorine species that appeared on the NaCl surface when exposed to SO_2 . Core electron binding energy (CEBE) calculations were performed for different chlorine species adsorbed on the surface of a NaCl ionic and cubic crystal slab with two open gas/crystal interfaces (see the [Supporting Information](#) for full details on the computational methodology). The considered compounds were Cl^\bullet (Cl radical), Cl_2 , HCl , HSO_3Cl , NCl_3 , NH_2Cl , SCl_2 , and SO_2Cl_2 . For the sake of efficient screening and as a result of the computational cost of the calculations, a single molecule was placed on the surface of the crystal at one time, as shown in [Figure S3](#) of the [Supporting Information](#). In addition, we tested the effect of the adsorption of hydronium (H_3O^+) and hydroxyl (OH^-) ions on the CEBE of interfacial Cl atoms belonging to crystal NaCl (panels b and c of [Figure S3](#) of the [Supporting Information](#)). [Table S1](#) of the [Supporting Information](#) shows that, for all considered species, the Cl 2p lines lie at higher BE than those corresponding to Cl atoms belonging to the crystal substrate, indicating that none of them is the species responsible for the doublet at lower BE in [Figure 1b](#). Moreover, this finding agrees with the general idea that CEBE increases when valence electrons are involved in bonds, because they reduce screening of nuclei attraction on the core electrons.²⁸

Computational results help to clarify the replacement of chloride by sulfate at the surface of the NaCl crystal while also explaining the nature of the low BE doublet observed in [Figure 1a](#). [Figure S4](#) of the [Supporting Information](#) shows the energy profile obtained by the energy elastic band (see the [Supporting Information](#) for details) for the interfacial chloride–sulfate replacement. Interestingly, the BE of Cl atoms in the ionic lattice is higher than that of Cl^- ions expelled from the crystal (violet atom in the black and red insets of [Figure S4](#) of the [Supporting Information](#), respectively). This difference ([Table S1](#) of the [Supporting Information](#)) is 2.2 eV, close to the experimental observation (about 1.6 eV). Generally, the BE of the core electrons increases when the valence electrons are involved in bonds,²⁸ and the higher BE for Cl^- core electrons in the crystal may be due to a certain degree of electron sharing that is always present also in ionic bonds. This sharing reduces the screening of the valence electrons on the nuclei–core electron interaction, increasing the BE of core electrons in the crystal. On the other hand, when chloride is isolated, the screening of the valence electrons on the nucleus interaction is more effective, and thus, BE of core electrons is lower than in

the mineral case. [Figure S4](#) of the [Supporting Information](#) also shows a significant restructuring of the NaCl lattice and a very high energy barrier for the chloride–sulfate replacement in the absence of water. Interfacial dissolution of the NaCl crystal occurs in the presence of water,²⁹ and the adsorption of few water molecules, even at low RH, are very likely to catalyze the interfacial chloride–sulfate substitution, lowering the high energy barrier for the chloride–sulfate replacement observed in [Figure S4](#) of the [Supporting Information](#) in the absence of water.

To provide a molecular picture of the sub-monolayer solvation of the NaCl crystal, we performed 60 ps FPMD at 300 K, by placing 12 water molecules, 1 H_2SO_4 , 1 H_2SO_3 , 1 HCl , 1 Na_2SO_4 , and 1 SO_2 on the mineral surface (details in the [Supporting Information](#)). This system composition aims to resemble a possible scenario that may have been observed experimentally at low RH, with a water sublayer deposited on the surface of the crystals. Simulations show the ordering of water molecules in proximity to the water surface, a hectic proton dynamic, the formation of hydrogen bonds between water and solutes, hydroxyl and hydronium ions, and ion pairing ([Figure S5](#) of the [Supporting Information](#)). Interestingly, the formation of hydroxyl and hydronium ions has also been reported at the interface of fully water-solvated NaCl crystals.³⁰ Here, inspection of the trajectory surprisingly reveals spontaneous dehydration of sulfurous acid into SO_2 ([Figure 4a](#)). Taken together, the simulations indicate that the partially solvated interfacial region of the crystalline surface is a very chemically active environment. A reason could be that, at the proximity of the mineral/water solution interface, solutes and solvent molecules are subject to an intense electric field, which may catalyze reactions.^{31,32} [Figure 4b](#) shows the average component of the electric field along the direction (z) perpendicular to the crystal interface; the electric field profile shows two intense peaks, one localized at the mineral interface and one at the adsorbed water layer, while the electric field vanishes moving into the gas phase. The intensity of these peaks is 2.5 and 2 V/Å, respectively. The features shown in [Figure 4b](#) resemble those observed on other mineral–water interfaces,³¹ even if, in the present case, the high concentration and particular composition of the ionic species in the adsorbed water sub-monolayer play a substantial role in modulating the interfacial field. Nevertheless, it is crucial to note that, at the adsorbed water layer, the intensity of the electric field exceeds the value of 0.35 V/Å, at which water autoionizes.^{33,34} This very likely explains the hectic proton dynamics and reactivity of such an environment and also the spontaneous oxidation of SO_2 on the NaCl surface without conventional oxidizing

molecules observed experimentally. It is worth mentioning that, in the limited simulation time of computationally expensive FPMD, it was impossible to record the occurrence of Cl–sulfate replacement. Computational FPMD studies in the literature on the dissolution of a fully solvated NaCl crystal reported that more than 100 ps are needed to observe the initial disruption of the mineral lattice.²⁹ In addition, the reactions were accelerated in the experiments by X-ray radiation, which is not considered in the simulation.

The results from this study show that salt surfaces can be reactive environments, providing the possibility for unconventional reactions under certain circumstances. The surface of NaCl is found to have a strong electric field, which is enough to autoionize water molecules. Such specific surface properties may explain the high chemical reactivities and SO₂ uptake on chloride salts, especially on NaCl.

■ ASSOCIATED CONTENT

SI Supporting Information

The Supporting Information is available free of charge at <https://pubs.acs.org/doi/10.1021/acs.jpclett.3c00980>.

Materials and methods, chemometric analysis, experimental temperature and pressure, effects of soft X-ray on chloride–sulfate replacement, oxygen K-edge NEXAFS of NH₄Cl, relative sulfur abundance, and computational methodology (PDF)

Transparent Peer Review report available (PDF)

■ AUTHOR INFORMATION

Corresponding Authors

Xiangrui Kong – Department of Chemistry and Molecular Biology, Atmospheric Science, University of Gothenburg, 41296 Gothenburg, Sweden; orcid.org/0000-0002-7205-0723; Email: kongx@chem.gu.se

Ivan Gladich – European Centre for Living Technology (ECLT), 30124 Venice, Italy; Qatar Environment and Energy Research Institute, Hamad Bin Khalifa University, Doha, Qatar; orcid.org/0000-0003-0929-3439; Email: igladich@hbku.edu.qa

Jan B. C. Pettersson – Department of Chemistry and Molecular Biology, Atmospheric Science, University of Gothenburg, 41296 Gothenburg, Sweden; orcid.org/0000-0001-8420-6126; Email: janp@chem.gu.se

Authors

Nicolas Fauré – Department of Chemistry and Molecular Biology, Atmospheric Science, University of Gothenburg, 41296 Gothenburg, Sweden; orcid.org/0000-0003-3200-2337

Erik S. Thomson – Department of Chemistry and Molecular Biology, Atmospheric Science, University of Gothenburg, 41296 Gothenburg, Sweden; orcid.org/0000-0003-2428-7539

Jie Chen – Department of Environmental Systems Science, ETH Zürich, 8092 Zürich, Switzerland

Luca Artiglia – Laboratory of Atmospheric Chemistry, Paul Scherrer Institute, 5232 Villigen PSI, Switzerland; orcid.org/0000-0003-4683-6447

Markus Ammann – Laboratory of Atmospheric Chemistry, Paul Scherrer Institute, 5232 Villigen PSI, Switzerland; orcid.org/0000-0001-5922-9000

Thorsten Bartels-Rausch – Laboratory of Atmospheric Chemistry, Paul Scherrer Institute, 5232 Villigen PSI, Switzerland; orcid.org/0000-0002-7548-2572

Zamin A. Kanji – Department of Environmental Systems Science, ETH Zürich, 8092 Zürich, Switzerland; orcid.org/0000-0001-8610-3921

Complete contact information is available at: <https://pubs.acs.org/doi/10.1021/acs.jpclett.3c00980>

Notes

The authors declare no competing financial interest.

■ ACKNOWLEDGMENTS

This project is supported by the Swedish Research Council under Contract 2021-04042. Xiangrui Kong and Erik S. Thomson acknowledge the support from the Swedish Foundation for International Cooperation in Research and Higher Education (CH2019-8361). Erik S. Thomson and Nicolas Fauré have also been supported by the Swedish Research Council VR (2020-03497). For high-performance computing (HPC) resources and services, the authors acknowledge the Research Computing Group in Texas A&M University at Qatar, founded by the Qatar Foundation for Education, Science and Community Development, and the use of Qatar Environment and Energy Research Institute (QEERI) HPC under Project ID HPC-P21002. Ivan Gladich thanks Prof. Kari Laasonen and Dr. Rasmus Kronberg for insightful discussions about the simulation setup of the NaCl crystal.

■ REFERENCES

- (1) Xie, C.; Niu, Z.; Kim, D.; Li, M.; Yang, P. Surface and interface control in nanoparticle catalysis. *Chem. Rev.* **2020**, *120* (2), 1184–1249.
- (2) Kong, X.; Castarede, D.; Thomson, E. S.; Boucly, A.; Artiglia, L.; Ammann, M.; Gladich, I.; Pettersson, J. B. C. A surface-promoted redox reaction occurs spontaneously on solvating inorganic aerosol surfaces. *Science* **2021**, *374* (6568), 747–752.
- (3) Martínez-Pabello, P. U.; Navarro-González, R.; Walls, X.; Pi-Puig, T.; González-Chávez, J. L.; de la Rosa, J. G.; Molina, P.; Zamora, O. Production of nitrates and perchlorates by laser ablation of sodium chloride in simulated Martian atmospheres. Implications for their formation by electric discharges in dust devils. *Life Sci. Space Res.* **2019**, *22*, 125–136.
- (4) Poston, M. J.; Carlson, R. W.; Hand, K. P. Spectral behavior of irradiated sodium chloride crystals under Europa-like conditions. *J. Geophys. Res.: Planet* **2017**, *122* (12), 2644–2654.
- (5) Ye, C.; Glotch, T. D. Spectral properties of chloride salt-bearing assemblages: Implications for detection limits of minor phases in chloride-bearing deposits on Mars. *J. Geophys. Res.: Planet* **2019**, *124* (2), 209–222.
- (6) Zieger, P.; Väisänen, O.; Corbin, J. C.; Partridge, D. G.; Bastelberger, S.; Mousavi-Fard, M.; Rosati, B.; Gysel, M.; Krieger, U. K.; Leck, C.; Nenes, A.; Riipinen, I.; Virtanen, A.; Salter, M. E. Revising the hygroscopicity of inorganic sea salt particles. *Nat. Commun.* **2017**, *8* (1), 15883.
- (7) Bartels-Rausch, T.; Kong, X.; Orlando, F.; Artiglia, L.; Waldner, A.; Huthwelker, T.; Ammann, M. Interfacial supercooling and the precipitation of hydrohalite in frozen NaCl solutions as seen by X-ray absorption spectroscopy. *Cryosphere* **2021**, *15* (4), 2001–2020.
- (8) Wagner, R.; Möhler, O. Heterogeneous ice nucleation ability of crystalline sodium chloride dihydrate particles. *J. Geophys. Res. Atmos.* **2013**, *118* (10), 4610–4622.
- (9) Finlayson-Pitts, B. J. The tropospheric chemistry of sea salt: A molecular-level view of the chemistry of NaCl and NaBr. *Chem. Rev.* **2003**, *103* (12), 4801–4822.

- (10) Wise, M. E.; Martin, S. T.; Russell, L. M.; Buseck, P. R. Water uptake by NaCl particles prior to deliquescence and the phase rule. *Aerosol Sci. Technol.* **2008**, *42* (4), 281–294.
- (11) Robinson, E.; Robbins, R. C. Gaseous sulfur pollutants from urban and natural sources. *J. Air Pollut. Control Assoc.* **1970**, *20* (4), 233–235.
- (12) Fioletov, V. E.; McLinden, C. A.; Krotkov, N.; Li, C. Lifetimes and emissions of SO₂ from point sources estimated from OMI. *Geophys. Res. Lett.* **2015**, *42* (6), 1969–1976.
- (13) Wang, Y.; Zhang, Q.; Jiang, J.; Zhou, W.; Wang, B.; He, K.; Duan, F.; Zhang, Q.; Philip, S.; Xie, Y. Enhanced sulfate formation during China's severe winter haze episode in January 2013 missing from current models. *J. Geophys. Res.: Atmos.* **2014**, *119* (17), 10,425–10,440.
- (14) Seinfeld, J. H.; Pandis, S. N. *Atmospheric Chemistry and Physics: From Air Pollution to Climate Change*; John Wiley & Sons, Inc.: Hoboken, NJ, 2016.
- (15) Liu, T.; Chan, A. W. H.; Abbatt, J. P. D. Multiphase oxidation of sulfur dioxide in aerosol particles: Implications for sulfate formation in polluted environments. *Environ. Sci. Technol.* **2021**, *55* (8), 4227–4242.
- (16) Zheng, B.; Zhang, Q.; Zhang, Y.; He, K. B.; Wang, K.; Zheng, G. J.; Duan, F. K.; Ma, Y. L.; Kimoto, T. Heterogeneous chemistry: A mechanism missing in current models to explain secondary inorganic aerosol formation during the January 2013 haze episode in North China. *Atmos. Chem. Phys.* **2015**, *15* (4), 2031–2049.
- (17) IPCC, 2021: Summary for Policymakers. In *Climate Change 2021: The Physical Science Basis. Contribution of Working Group I to the Sixth Assessment Report of the Intergovernmental Panel on Climate Change*; Masson-Delmotte, V.; Zhai, P.; Pirani, A.; Connors, S. L.; Péan, C.; Berger, S.; Caud, N.; Chen, Y.; Goldfarb, L.; Gomis, M. L.; Huang, M.; Leitzell, K.; Lonnoy, E.; Matthews, J. B. R.; Maycock, T. K.; Waterfield, T.; Yelekçi, O.; Yu, R.; Zhou, B., Eds.; Cambridge University Press: Cambridge, U.K., 2021.
- (18) Ruiz-Lopez, M. F. Midair transformations of aerosols. *Science* **2021**, *374* (6568), 686–687.
- (19) Gladich, I.; Lin, C.; Sinopoli, A.; Francisco, J. S. Uptake and hydration of sulfur dioxide on dry and wet hydroxylated silica surfaces: A computational study. *Phys. Chem. Chem. Phys.* **2021**, *24* (1), 172–179.
- (20) Tissot, H.; Olivieri, G.; Gallet, J.-J.; Bournel, F.; Silly, M. G.; Sirotti, F.; Rochet, F. Cation depth-distribution at alkali halide aqueous solution surfaces. *J. Phys. Chem. C* **2015**, *119* (17), 9253–9259.
- (21) Peisert, H.; Chassé, T.; Streubel, P.; Meisel, A.; Szargan, R. Relaxation energies in XPS and XAES of solid sulfur compounds. *J. Electron. Spectrosc.* **1994**, *68*, 321–328.
- (22) Fantauzzi, M.; Elsener, B.; Atzei, D.; Rigoldi, A.; Rossi, A. Exploiting XPS for the identification of sulfides and polysulfides. *RSC Adv.* **2015**, *5* (93), 75953–75963.
- (23) Fauré, N.; Chen, J.; Artiglia, L.; Ammann, M.; Bartels-Rausch, T.; Li, J.; Liu, W.; Wang, S.; Kanji, Z. A.; Pettersson, J. B. C.; Gladich, I.; Thomson, E. S.; Kong, X. Unexpected behavior of chloride and sulfate ions upon surface solvation of Martian salt analogue. *ACS Earth Space Chem.* **2023**, *7* (2), 350–359.
- (24) Baltrusaitis, J.; Usher, C. R.; Grassian, V. H. Reactions of sulfur dioxide on calcium carbonate single crystal and particle surfaces at the adsorbed water carbonate interface. *Phys. Chem. Chem. Phys.* **2007**, *9* (23), 3011–3024.
- (25) Prado, R. J.; M. Flank, A. Sodium K-Edge XANES calculation in 'NaCl' type structures. *Phys. Scr.* **2005**, *2005* (T115), 165.
- (26) Zelenay, V.; Ammann, M.; Křepelová, A.; Birrer, M.; Tzvetkov, G.; Vernooij, M. G. C.; Raabe, J.; Huthwelker, T. Direct observation of water uptake and release in individual submicrometer sized ammonium sulfate and ammonium sulfate/adipic acid particles using X-ray microspectroscopy. *J. Aerosol Sci.* **2011**, *42* (1), 38–51.
- (27) Tanuma, S.; Powell, C. J.; Penn, D. R. Calculations of electron inelastic mean free paths. V. Data for 14 organic compounds over the 50–2000 eV range. *Surf. Interface Anal.* **1994**, *21* (3), 165–176.
- (28) Tardio, S.; Cumpson, P. J. Practical estimation of XPS binding energies using widely available quantum chemistry software. *Surf. Interface Anal.* **2018**, *50* (1), 5–12.
- (29) Holmberg, N.; Chen, J.-C.; Foster, A. S.; Laasonen, K. Dissolution of NaCl nanocrystals: An ab initio molecular dynamics study. *Phys. Chem. Chem. Phys.* **2014**, *16* (33), 17437–17446.
- (30) Kronberg, R.; Laasonen, K. Dynamics and surface propensity of H⁺ and OH[−] within rigid interfacial water: Implications for electrocatalysis. *J. Phys. Chem. Lett.* **2021**, *12* (41), 10128–10134.
- (31) Laporte, S.; Finocchi, F.; Paulatto, L.; Blanchard, M.; Balan, E.; Guyot, F.; Saitta, A. M. Strong electric fields at a prototypical oxide/water interface probed by ab initio molecular dynamics: MgO(001). *Phys. Chem. Chem. Phys.* **2015**, *17* (31), 20382–20390.
- (32) Laporte, S.; Pietrucci, F.; Guyot, F.; Saitta, A. M. Formic acid synthesis in a water–mineral system: Major role of the interface. *J. Phys. Chem. C* **2020**, *124* (9), 5125–5131.
- (33) Cassone, G.; Sponer, J.; Trusso, S.; Saija, F. Ab initio spectroscopy of water under electric fields. *Phys. Chem. Chem. Phys.* **2019**, *21* (38), 21205–21212.
- (34) Saitta, A. M.; Saija, F.; Giaquinta, P. V. Ab Initio molecular dynamics study of dissociation of water under an electric field. *Phys. Rev. Lett.* **2012**, *108* (20), No. 207801.